

Reverberation Chamber Measurement Correlation

Ryan J. Pirkl, *Member, IEEE*, Kate A. Remley, *Senior Member, IEEE*, and Christian S. Lötbäck Patané

Abstract—This contribution evaluates the utility of several different metrics for studying correlation between reverberation chamber measurements collected at different stirrer positions. Metrics considered are the autocovariance, the correlation matrix, and two metrics based upon the entropy of the data correlation matrix: 1) the effective number of uncorrelated measurements and 2) the measurement efficiency. The different metrics are shown to be useful for different correlation analyses. Application of these metrics reveals that the correlation between reverberation chamber measurements is strongly affected by stirring methodology, loading configuration, and measurement frequency.

Index Terms—Correlation, entropy, measurement correlation, measurement efficiency, reverberation chamber.

I. INTRODUCTION

REVERBERATION chambers provide a statistical field distribution for measuring antenna radiation efficiency [1], electromagnetic susceptibility [2], and the performance of wireless communication systems [3]–[6]. However, correlation among measurements taken in a reverberation chamber severely degrades both the efficiency of the measurement procedure (e.g., due to oversampling) and the accuracy of the target measurement quantity (e.g., due to an insufficient number of effectively uncorrelated measurements). Here, we present several tools for studying correlation between reverberation chamber measurements at different stirrer positions and illustrate how these tools may be used to identify and mitigate correlation through improved experiment design.

To date, most investigations of reverberation chamber measurement correlation have focused solely on the autocovariance (or autocorrelation) of the measurement data with respect to a mechanical stirrer's position or angle. Typically, stirrer autocovariances have been used to determine the minimum stirrer displacement or rotation required to obtain uncorrelated measurements so as to estimate the maximum obtainable number of uncorrelated measurements [7]–[12] or to optimize the geometry of a mechanical stirrer [9], [13]. Taking a slightly different approach, [10], [14], [15] fit analytic models to the stirrer's autocovariance to compute an effective sample size for their measurements. In [10], this was used for uncertainty analysis,

whereas in [14], [15] it was used to compute an ideal stirrer stepsize.

Here we compare and contrast the utility of four metrics useful for evaluating different aspects of reverberation chamber measurement correlation: the autocovariance, the correlation matrix, the effective number of uncorrelated measurements, and measurement efficiency. We show that the autocovariance is an extremely practical, albeit specialized, tool for assessing *serial* correlation, i.e., correlation between sequential uniformly sampled measurements. This makes the autocovariance useful for characterizing the performance of individual stirrers [9], [13], but limits its ability to assess other manifestations of measurement correlation. The correlation matrix has been used previously for studying serial measurement correlation [14], but its true utility lies in its ability to facilitate the identification of correlation sources and the design of better stirring methodologies. The effective number of uncorrelated measurements distills a measurement dataset's correlation down to a single scalar value that quantifies the amount of unique information obtained from a set of measurements. This enables quantitative comparisons of different measurement configurations and a straightforward uncertainty analysis. Finally, measurement efficiency provides a succinct and intuitive assessment of one's measurement methodology that facilitates measurement optimization.

Discussion begins in Section II with a brief overview of the reverberation chamber measurements used to demonstrate the different correlation metrics. Then, in Sections III–VI we present the different correlation metrics and accompanying example calculations using various reverberation chamber measurement datasets. These example calculations demonstrate the utility of the different metrics and lead to the identification of several sources of reverberation chamber measurement correlation. In Section VII, we convert the insight afforded by these correlation metrics into practical guidelines for mitigating measurement correlation. Conclusions and future work are discussed in Section VIII.

II. REVERBERATION CHAMBER MEASUREMENTS

Measurements were taken in a 3.60 m by 4.27 m by 2.90 m reverberation chamber that used a pair of rotating mechanical paddles to “stir” the electromagnetic fields. The two orthogonal stirrer axes were positioned near, and oriented parallel to, two nonadjacent edges of the chamber. The first stirrer rotated about a vertical axis within a cylindrical volume 2.46 m high and 1.00 m in diameter. The second stirrer rotated about a horizontal axis within a cylindrical volume 3.3 m long and 1.00 m in diameter. Note that the length of the second stirrer was about 1.3 times the first. Stepped-paddle measurements were conducted, and the angular resolution of each stirrer was 0.1° . The measurements used a pair of 1 GHz to 18 GHz double-ridge guide

Manuscript received January 18, 2011; revised June 23, 2011; accepted August 16, 2011. Date of publication October 6, 2011; date of current version June 15, 2012. Work of the U.S. government, not subject to copyright.

R. J. Pirkl and K. A. Remley are with the National Institute of Standards and Technology, Electromagnetics Division, RF Fields Group, 325 Broadway St, MS 818.02, Boulder, CO 80305 USA (e-mail: ryan.pirkl@nist.gov; kate.remley@nist.gov).

C. S. L. Patané is with Bluetest AB, Götaverksgatan 1, SE-417 55 Gothenburg, Sweden (e-mail: c.lotback@gmail.com).

Color versions of one or more of the figures in this paper are available online at <http://ieeexplore.ieee.org>.

Digital Object Identifier 10.1109/TEMC.2011.2166964

horn antennas that were cross-polarized and pointed away from each other and toward the two mechanical stirrers. The antennas were connected to a vector network analyzer (VNA), which was calibrated at the antenna ports. For each of the N different stirrer positions, the VNA was used to record the complex S_{21} at $M = 16,001$ equispaced frequencies from 0.8 GHz to 6 GHz. The VNA manufacturer's specified uncertainty in the measured S_{21} 's magnitude and phase were 0.2 dB and 1° , respectively. The technique described in [16] was used to correct for antenna impedance mismatches. The resulting dataset was compiled into a M -by- N data matrix, \mathbf{H} , given by

$$\mathbf{H} = \begin{bmatrix} h_1(f_1) & h_2(f_1) & \cdots & h_N(f_1) \\ h_1(f_2) & h_2(f_2) & \cdots & h_N(f_2) \\ \vdots & \vdots & \ddots & \vdots \\ h_1(f_M) & h_2(f_M) & \cdots & h_N(f_M) \end{bmatrix} \quad (1)$$

where the matrix element $h_n(f_m)$ denotes the mismatch-corrected complex S_{21} measurement corresponding to the m th frequency f_m and n th stirrer position.

A. Stirrer Rotation Algorithms

Three different mechanical stirrer rotation algorithms were tested to study the effect of relative paddle position on measurement correlation. In later sections, we use our correlation analyses to compare the effectiveness of these different algorithms and gain insight into stirrer rotation algorithm design. In the following discussion, $\phi_1 \in [0^\circ, 360^\circ)$ denotes the angle of the first mechanical stirrer, and $\phi_2 \in [0^\circ, 360^\circ)$ denotes the angle of the second mechanical stirrer.

1) *Uniform Linear*: $(\Delta\phi_1, \Delta\phi_2)$: For the uniform linear algorithm, the stirrers were rotated by some fixed angle pair, $(\Delta\phi_1, \Delta\phi_2)$, whereby, for each new measurement, the first stirrer was rotated by $\Delta\phi_1$ and the second stirrer was rotated by $\Delta\phi_2$. Fig. 1(a) illustrates the angles, ϕ_1 and ϕ_2 , of the two stirrers when using the uniform linear algorithm with various stirrer rotation angle pairs to obtain $N = 25$ measurements.

2) *Uniform Grid*: The uniform grid algorithm rotates the stirrers to the set of angle pairs, $\{(\phi_1, \phi_2)\}$, that lie on a rectangular grid in the ϕ_1 - ϕ_2 angle space. For the measurements discussed here, N was restricted to a perfect square whereby the grid dimensions were \sqrt{N} -by- \sqrt{N} with an intragrid spacing of $\Delta\phi_1 = \Delta\phi_2 = 360^\circ/\sqrt{N}$. Fig. 1(b) illustrates the angles, ϕ_1 and ϕ_2 , of the two stirrers when using the uniform grid algorithm to obtain $N = 25$ measurements.

3) *Maximin Distance*: For a set of N measurements, the maximin distance algorithm seeks two ordered sets, $\{\phi_1\}$ and $\{\phi_2\}$, each containing N unique stirrer angles such that the corresponding set of stirrer angle pairs, $\{(\phi_1, \phi_2)\}$, are uniformly distributed throughout the ϕ_1 - ϕ_2 angle space with a minimum separation distance in ϕ_1 or ϕ_2 of $360^\circ/N$. That is, the algorithm seeks to maximize the minimum distance between points in the ϕ_1 - ϕ_2 angle space while also ensuring that each stirrer's set of N angles is unique. Rather than directly solving the implicit maximin optimization problem, we opt for an efficient heuristic

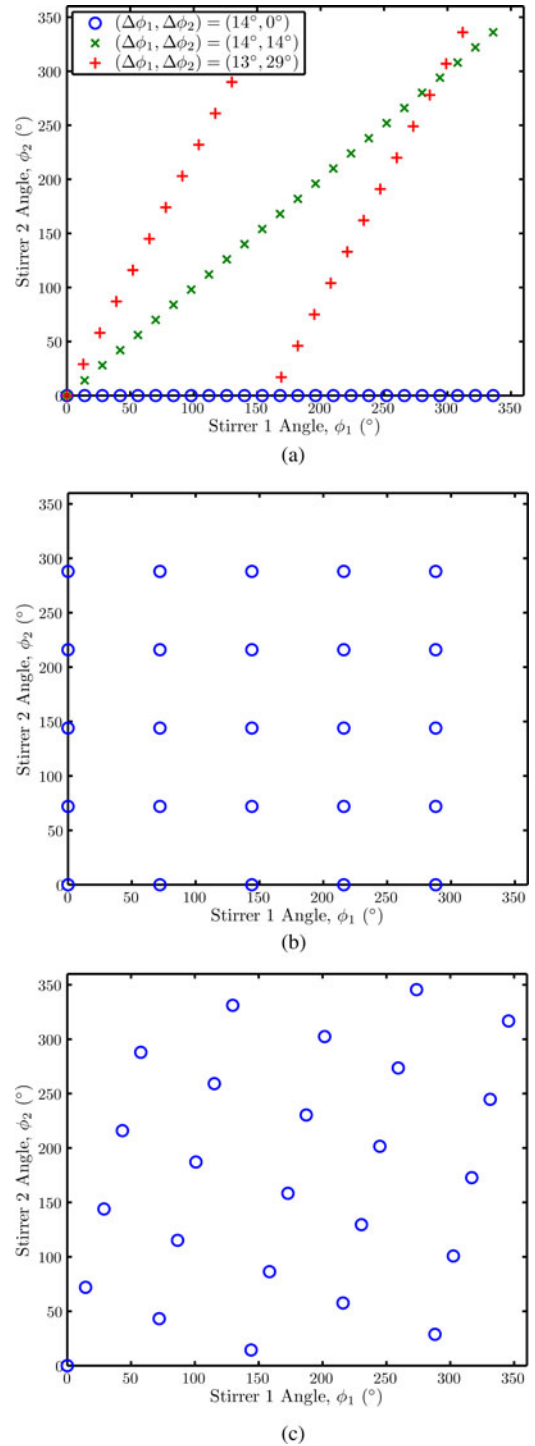


Fig. 1. Diagram of the stirrer angles, (ϕ_1, ϕ_2) , attained by use of three different stirrer rotation algorithms for $N = 25$ measurements: (a) uniform linear, (b) uniform grid, (c) maximin distance.

solution that yields a pair of ordered angle sets, $\{\phi_1\}$ and $\{\phi_2\}$, exhibiting approximately uniform separation in angle space. Details of this heuristic solution are presented in Appendix A. Fig. 1(c) illustrates the angles, ϕ_1 and ϕ_2 , of the two stirrers when this maximin distance algorithm is used to obtain $N = 25$ measurements.

III. AUTOCOVARANCE

The autocovariance is a measure of the correlation between an observed signal and a shifted or delayed copy of itself. Given the periodicity of our reverberation chamber measurement data, which arises due to our use of rotating mechanical stirrers, we opt to use a circular autocovariance given by [17]

$$\rho_h(f_m, \Delta n) = \frac{\langle h_n(f_m) h_{n+\Delta n}^*(f_m) \rangle_n - |\langle h_n(f_m) \rangle_n|^2}{\langle |h_n(f_m)|^2 \rangle_n - |\langle h_n(f_m) \rangle_n|^2} \quad (2)$$

where $\Delta n \in [0, N - 1]$, the index $n + \Delta n$ is computed by use of modulo N arithmetic, $\langle \cdot \rangle_n$ denotes the ensemble average taken across all stirrer positions, and \cdot^* denotes the complex conjugate. Implicitly, we are assuming that the stirrer-dependent fluctuations of S_{21} may be modelled as a wide-sense stationary process.

In [9], [13], stirrer performance analyses were conducted using an autocovariance similar to (2). It is worth pointing out that, unlike the autocorrelation, the autocovariance removes the mean of the signal and is thus a generally applicable measure of correlation. In contrast, the autocorrelation is only a valid correlation measure when the data has a mean of zero. This distinction is particularly important for reverberation chamber measurements, wherein the measurement configuration may lead to a Rician-type environment characterized by a nonzero and frequency-dependent average S_{21} [18]. Of course, for cases where the Rician K-factor is zero, the autocovariance and autocorrelation are identical.

For our analysis, we will use a frequency-averaged circular autocovariance given by

$$\rho_h(\Delta n) = \langle \rho_h(f_m, \Delta n) \rangle_f \quad (3)$$

where $\langle (\cdot) \rangle_f$ denotes an ensemble average taken over some bandwidth. Due to the additional frequency averaging, (3) provides a better estimate of the stirrer's correlation function than (2).

Fig. 2 presents examples of two circular stirrer autocovariances frequency-averaged over a 1 GHz bandwidth centered around 2 GHz. The 1 GHz frequency-averaging bandwidth was chosen so as to be consistent with results presented in Section V, wherein a 1 GHz bandwidth is necessary to accurately estimate the same datasets' effective number of uncorrelated measurements, N_{eff} . The autocovariances were calculated from reverberation chamber measurement datasets that used a three-absorber loading configuration and the uniform linear stirring algorithm with $N = 360$, whereby $\Delta n = 1$ in (2)–(3) corresponds to $\Delta\phi = 1^\circ$. The uncertainty in the autocovariance traces was determined by combining the uncertainty in (3)'s ensemble average across frequency with the uncertainty arising due to the 0.1° resolution of the stirrer rotation angles. For the latter uncertainty contribution, we equated the uncertainty in the stirrer rotation angle with the stirrers' 0.1° resolution and propagated this uncertainty through $\rho_h(\Delta n)$. The resulting combined uncertainty was dominated by the 0.1° resolution of the stirrer rotation angles and was determined to be less than 0.025. Comparing the autocovariances in Fig. 2, it may be seen that

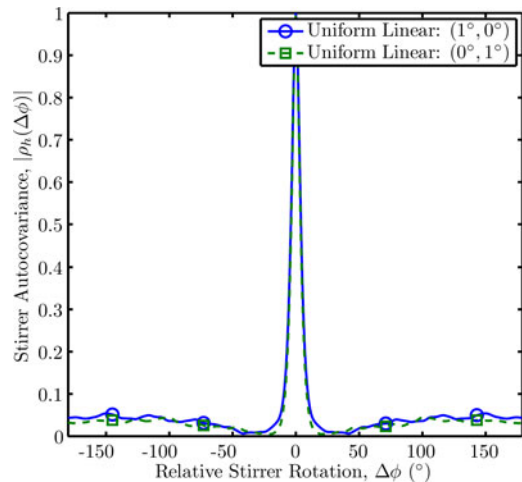


Fig. 2. Frequency-averaged circular autocovariance calculated with respect to stirrer angle for $N = 360$ measurements. The autocovariance was averaged across a 1 GHz bandwidth centered around 2 GHz.

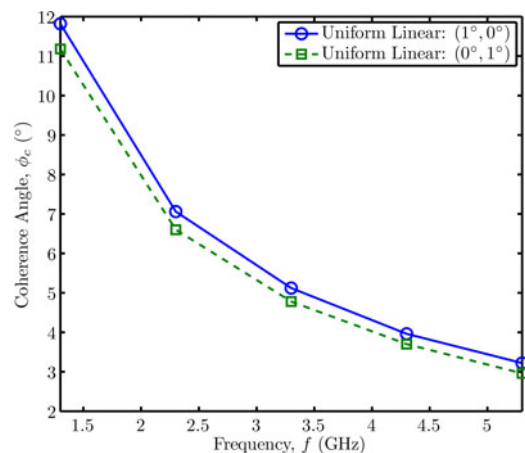


Fig. 3. Coherence angle ϕ_c as a function of frequency.

they exhibit similar trends, including a single peak at $\Delta\phi = 0^\circ$, which indicates that the mechanical stirrers have only one angle of rotational symmetry corresponding to 360° .

A. Coherence Angle/Distance

An autocovariance with respect to stirrer orientation/position may be used to determine the stirrer's *coherence angle/distance*, which describes how far the stirrer should be rotated/displaced to obtain a new measurement having a specified level of correlation [7], [8], [11]. These coherence metrics may be defined by the width of the normalized autocovariance at some threshold correlation value. Here, we use a threshold of 0.5, whereby the coherence angle, denoted ϕ_c , corresponds to the normalized autocovariance's full-width at half-maximum.

Fig. 3 presents example calculations of the coherence angle ϕ_c as a function of frequency for the same datasets used to calculate the autocovariances in Fig. 2. The corresponding stirrer autocovariances were again frequency-averaged over a 1 GHz bandwidth. The relative uncertainty in the calculation of the coherence angles was due to a combination of the stirrer rotation

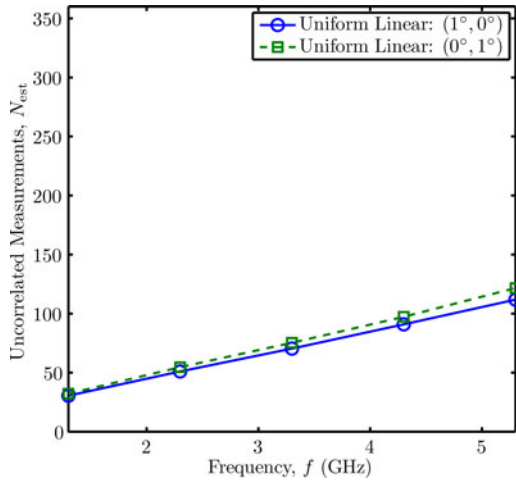


Fig. 4. Estimated number of uncorrelated measurements N_{est} as determined by the coherence angle ϕ_c from a set of $N = 360$ measurements taken at 1° intervals.

angle resolution and the uncertainty in the autocovariances and was determined to be less than 5%. Fig. 3 reveals that the coherence angle tends to decrease with increasing frequency. This indicates that lower frequencies (i.e., larger wavelengths) require larger stirrer rotations to decorrelate the measurements [8], [19]. Comparing the performance of the individual stirrers, the second stirrer (dashed trace) yields a consistently smaller coherence angle than the first (solid trace). In Section II, we noted that the second stirrer was slightly larger than the first stirrer. Thus, the second stirrer's superior performance may be attributed to its larger geometry.

B. Estimated Number of Uncorrelated Measurements

Provided that measurements at coherence angles ϕ_c are sufficiently decorrelated, one may use the coherence angle to estimate the total number of uncorrelated measurements that may be obtained from a single stirrer [7], [8], [11]. This estimate, denoted N_{est} , is given by

$$N_{\text{est}} = \frac{360^\circ}{\phi_c}. \quad (4)$$

Fig. 4 presents example calculations of the estimated number of uncorrelated measurements based on the coherence angles ϕ_c presented in Fig. 3. By propagating the uncertainty in the coherence angles through (4), the relative uncertainty in N_{est} was determined to be less than 5%. Fig. 4 reveals that only a small subset of the $N = 360$ measurements were uncorrelated. In other words, Figs. 3 and 4 indicate that taking measurements at 1° increments amounts to an oversampling of the reverberation chamber's wireless channel with respect to stirrer angle.

In general, the stirrer autocovariance provides a useful tool for determining how far to move or rotate a stirrer in order to minimize the correlation between measurements. This makes the autocovariance an invaluable tool for evaluating the performance of an individual stirrer. However, it is not the best tool for assessing the correlation between arbitrary measurement pairs nor for evaluating the effectiveness of one's mea-

surement methodology, because an autocovariance is suitable only when sequential, uniform, and finely sampled stirrer rotations/displacements are used (e.g., the "Uniform Linear" stirrer rotation algorithm with sub-coherence-angle increments).

IV. CORRELATION MATRIX

The correlation matrix provides a far more general tool for evaluating the correlation between measurement pairs. For an N -by- N correlation matrix, \mathbf{R} , computed from an M' -by- N submatrix of the original data matrix, \mathbf{H} , the matrix element, r_{ij} , describing the correlation between the i th and j th stirrer positions and occupying the i th row and j th column of \mathbf{R} is given by [20]

$$r_{ij} = \frac{\sigma_{ij}}{\sqrt{\sigma_{ii}\sigma_{jj}}}. \quad (5)$$

In (5), σ_{ij} denotes the elements of the corresponding covariance matrix, Σ as given by [20]

$$\sigma_{ij} = \frac{1}{M' - 1} \sum_{m=m'}^{m'+M'} \left\{ (h_i(f_m) - \langle h_i(f_m) \rangle_f) \times (h_j(f_m) - \langle h_j(f_m) \rangle_f)^* \right\}. \quad (6)$$

In (5)–(6), $i, j \in \{1, 2, \dots, N\}$ and the primed variables, m' and $M' \leq M$ are used to identify a bandwidth from which M' uncorrelated frequencies are used to calculate the covariance σ_{ij} . Here, uncorrelated frequencies are defined as those separated by a coherence bandwidth, B_c , as given by the full-width at half-maximum of a frequency domain autocorrelation [21]. Implicitly, the ensemble averages, $\langle h_i(f_m) \rangle_f$ and $\langle h_j(f_m) \rangle_f$, in (6) are frequency-averaged using this same set of M' frequencies.

Assuming the measurement data are complex Gaussian, the uncertainty in the elements of the sample correlation matrix is approximately $(1 - |r_{ij}|^2)/\sqrt{M' - 1}$ for large M' [22], whereby attaining an uncertainty of 0.05 can require $M' \approx 400$ uncorrelated observations (frequencies). Depending on the chamber's coherence bandwidth, this may necessitate a large calculation bandwidth, which, due to the inherent frequency dependence of the measurement data's insertion loss (see [18], [23]) and correlation (see Fig. 4), may obfuscate the interpretation of the resulting correlation matrix. To mitigate this issue, we row standardize the data matrix \mathbf{H} prior to estimating the covariance matrices. This forces the mean and variance of each row of \mathbf{H} to zero and one, respectively, such that each observation (frequency) is given equal weight in the calculation of the correlation matrix \mathbf{R} [24]. Nominally, the higher correlation at the lower bounds of the calculation bandwidth will be offset by the lower correlation at the upper bounds of the calculation bandwidth, whereby the frequency-averaged correlation matrix will reflect the measurement correlation near the calculation bandwidth's center. Of course, this cannot be guaranteed, but it does indicate that the implications of frequency-averaging the correlation matrix are less severe than one might initially suspect. The same comments apply to (3)'s frequency-averaged circular autocovariance. Finally, we note that row standardization also

resolves potential errors in the correlation matrix estimation for Rician distributed measurement data characterized by a nonzero row- (i.e., frequency-) dependent mean [25].

Fig. 5 presents example correlation matrix calculations for four different measurement datasets with $N = 100$ measurements and a three absorber loading configuration. The correlation matrices were calculated from the row-standardized measurement data within a 1 GHz bandwidth centered about 2 GHz and are presented using a logarithmic color scale to emphasize the different matrix structures. The 1 GHz bandwidth was used so as to be consistent with the results presented in other sections as well as to attain a reasonable uncertainty in the elements of the correlation matrix. From an analysis of the variance of the elements of the covariance matrices, the elements of the correlation matrices were determined to have an uncertainty of approximately 0.05, or $10^{-1.3}$.

The correlation matrices presented in Fig. 5 provide convenient graphical representations of the correlation between each of the N different measurements. As may be expected, all of the correlation matrices exhibit a maximum correlation of unity along the main diagonal. Off this main diagonal, the values of the correlation matrix are seen to depend on the stirrer rotation algorithm used to collect the measurement data. Fig. 5(a), which corresponds to the “Uniform Linear: $(3.6^\circ, 3.6^\circ)$ ” algorithm, exhibits a broad main diagonal that reveals strong correlation between adjacent stirrer positions. This is unsurprising given that Fig. 3 indicates the 3.6° stirrer rotation angle used in Fig. 5(a) is less than either stirrer’s coherence angle at 2 GHz. Figs. 5(b)–(d) exhibit faint diagonal bands of moderate correlation off the main diagonal. Fig. 5(c) also exhibits square patches of moderate correlation along the main diagonal. Both of these correlation artifacts correspond to a pair of stirrer positions wherein either the first or second stirrer was at a similar angle. For these cases, it is as if only one stirrer is being used to decorrelate the measurements.

Overall, the correlation matrix is an excellent tool for graphically and thus *qualitatively* evaluating the correlation in a measurement dataset. This makes the correlation matrix convenient for analyzing and identifying sources of correlation for a given stirrer rotation algorithm. Furthermore, whereas the autocovariance should really only be used to evaluate the performance of a single stirrer (e.g., by way of its coherence angle/distance), the general formulation of the correlation matrix makes it applicable to measurements collected using an arbitrary number of stirrers and *any* stirring methodology. However, because it is inherently a 2-D measure of correlation, the correlation matrix is neither well suited for drawing definitive conclusions about the overall correlation in a dataset nor for making quantitative comparisons across different datasets and/or frequencies.

V. EFFECTIVE NUMBER OF UNCORRELATED MEASUREMENTS

A more succinct correlation metric may be found by considering the total amount of information, or *entropy* in the measurement data. Intuitively, correlation among different measurements should result in redundant information that limits the maximum amount of information in N measurements. Thus,

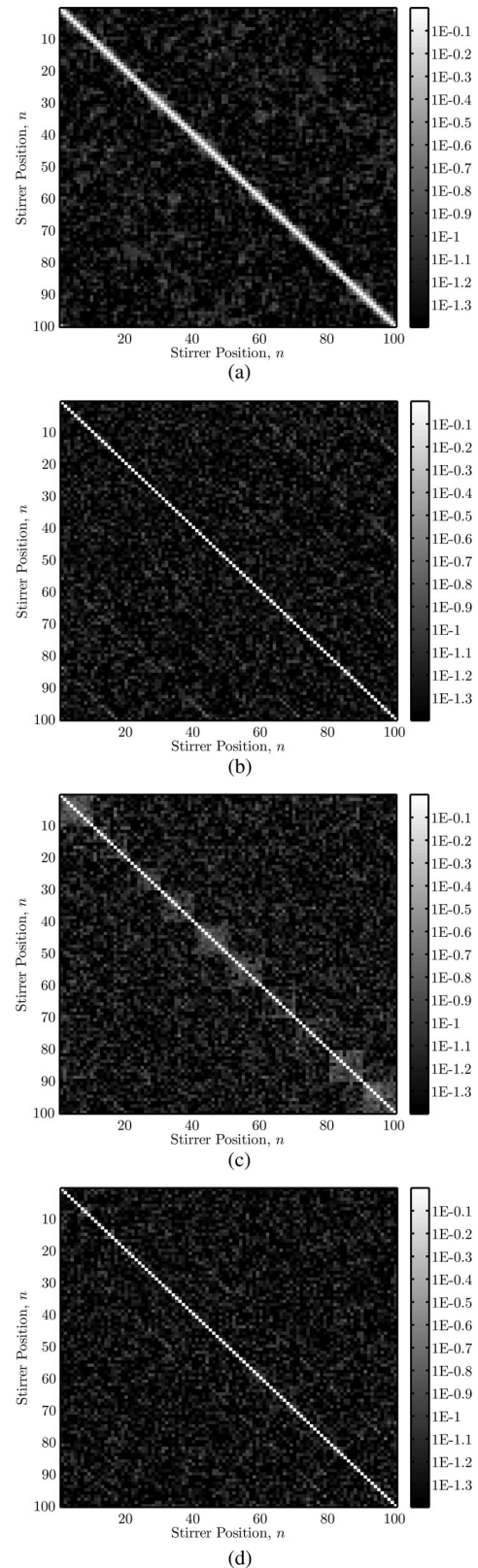


Fig. 5. Correlation matrices for different stirring algorithms with three absorbers and $N = 100$: (a) uniform linear: $(3.6^\circ, 3.6^\circ)$, (b) uniform linear: $(7^\circ, 13^\circ)$, (c) uniform grid, and (d) maximin distance.

the more correlated the measurement data, the more redundant information contained in the measurements, and the lower the measurement data's overall (i.e., joint) entropy.

For multivariate data akin to the data matrix \mathbf{H} , the conventional entropy metric is determined based on the distribution of the eigenvalues of the data's covariance matrix $\mathbf{\Sigma}$ [26], [27]. As in [28], [29], we consider a slight variation of this formulation based on the eigenvalues λ_n of the correlation matrix \mathbf{R}

$$I_\alpha = \frac{1}{1-\alpha} \ln \left(\sum_{n=1}^N \hat{\lambda}_n^\alpha \right) \quad (7)$$

where $\hat{\lambda}_n$ are the normalized eigenvalues of \mathbf{R} as given by

$$\hat{\lambda}_n = \frac{\lambda_n}{\sum_{n=1}^N \lambda_n}. \quad (8)$$

Equation (8) casts the spectrum of \mathbf{R} as a discrete probability distribution and (7) calculates this discrete distribution's Rényi entropy I_α of order α [30]. Values of I_α range from 0 for a single nonzero eigenvalue to $\ln N$ for N equal eigenvalues. We note that (7) in the limit $\alpha \rightarrow 1$ corresponds to the classic Shannon entropy formula [31]. Henceforth, we shall restrict ourselves to Rényi entropy of order $\alpha = 2$, which has been used in various disciplines to develop a measure of the dimensionality of a system or dataset [27], [31], [32].

Ideally, the reverberation chamber measurements at each of the N different stirrer positions will be perfectly uncorrelated such that $\mathbf{R} = \mathbf{I}$, where \mathbf{I} denotes the identity matrix. For this ideal case, all N eigenvalues of the correlation matrix will be identical, and (7) will yield the maximum possible entropy corresponding to $I_2 = \ln N$. Given that $I_2 = \ln N$ is the entropy for N uncorrelated measurements, we can determine an effective number of uncorrelated measurements, N_{eff} , for N potentially correlated measurements by requiring that

$$I_2 = \ln N_{\text{eff}}. \quad (9)$$

Taking the exponential of both sides of (9) yields an expression for the effective number of uncorrelated measurements, N_{eff}

$$N_{\text{eff}} = e^{I_2}. \quad (10)$$

Equation (10) determines the corresponding number of uncorrelated measurements that would have yielded the same amount of information as the N original measurements. If the N original measurements were perfectly uncorrelated, whereby $\mathbf{R} = \mathbf{I}$, then $N_{\text{eff}} = N$. If the N measurements were perfectly correlated (with equal variances) such that \mathbf{R} is a unit matrix (i.e., all 1s), then $N_{\text{eff}} = 1$. Thereby, N_{eff} provides a convenient metric for quantifying the amount of unique information in the N measurements. Quantities analogous to N_{eff} have been used in other disciplines to describe the effective number of different events [31], the number of probabilities, $\hat{\lambda}_n$, that are significantly greater than zero [32], and the effective number of degrees of freedom [27].

Substituting (7) and (8) into (10) yields

$$N_{\text{eff}} = \frac{\left(\sum_{n=1}^N \lambda_n \right)^2}{\sum_{n=1}^N \lambda_n^2}. \quad (11)$$

By relating the summations in (11) to the trace of the correlation matrix, \mathbf{R} , and its square, \mathbf{R}^2 , the effective number of uncorrelated measurements may alternatively be expressed as [27]

$$N_{\text{eff}} = \frac{N^2}{\sum_{i,j=1}^N |r_{ij}|^2} \quad (12)$$

where r_{ij} are again the elements of the correlation matrix, \mathbf{R} . In practice, (12) tends to be more convenient, because it does not require the calculation of the correlation matrix's eigenvalues.

A. Uncertainty in an Ensemble Power Average

In addition to its simple physical interpretation, the effective number of uncorrelated measurements N_{eff} also provides insight into the uncertainty in a power ensemble average of N potentially correlated realizations of a random variable. Let us assume a set of N potentially correlated realizations of a complex normally distributed random variable, X , with a mean of $\bar{X} = 0$ and variance of σ_X^2 , whereby the real and imaginary components of X are independent and identically normally distributed as $\text{Re}(X) \sim \mathcal{N}(0, \sigma_X^2/2)$ and $\text{Im}(X) \sim \mathcal{N}(0, \sigma_X^2/2)$, respectively. This is analogous to S_{21} measured in a well-stirred reverberation chamber. By specifying that X has units proportional to voltage, we may define $P = |X|^2$ as a new exponentially distributed random variable analogous to $|S_{21}|^2$ with units proportional to power [33].

The variance $\sigma_{\hat{P}}^2$ in an estimate \hat{P} of the mean power \bar{P} from a set of N realizations of P is [34, Eq. (A.10)]

$$\sigma_{\hat{P}}^2 = \frac{1}{N^2} \sum_{i,j=1}^N \sigma_{ij,P} \quad (13)$$

where $\sigma_{ij,P}$ denotes the covariance between the i th and j th realization of P . The covariance, $\sigma_{ij,P}$, may be related to the covariance, $\sigma_{ij,X}$, between the i th and j th realization of X according to [33]

$$\sigma_{ij,P} = |\sigma_{ij,X}|^2. \quad (14)$$

Given N_P uncorrelated realizations of P , it is well known that the variance of the average power $\sigma_{\hat{P}}^2$, is given by [34]

$$\sigma_{\hat{P}}^2 = \frac{\sigma_P^2}{N_P}. \quad (15)$$

Casting (13) into a form analogous to (15) allows us to define an effective number of uncorrelated power realizations, N_P , for the N potentially correlated measurements. Solving (15) for N_P , employing (14) and (13), and recognizing that $\sigma_{ij,X} = \sigma_X^2$ for $i = j$ such that $\sigma_P^2 = \sigma_X^4$, the effective number of uncorrelated power measurements, N_P , may be expressed in terms of the covariance of the N realizations of X :

$$N_P = \frac{\frac{1}{N} \sum_{i=1}^N \sigma_X^4}{\frac{1}{N^2} \sum_{i,j=1}^N |\sigma_{ij,X}|^2}. \quad (16)$$

Multiplying the numerator and denominator by N^2/σ_X^4 and using (5) with $\sigma_{ii} = \sigma_{jj} = \sigma_X^2$ yields

$$N_P = \frac{N^2}{\sum_{i,j=1}^N |r_{ij}|^2} \quad (17)$$

which is *identical* to the expression for N_{eff} in (12). Substituting N_{eff} for N_P in (15) and taking the square root yields the *standard error* (see [34]) in the estimate of mean power:

$$\sigma_{\hat{P}} = \frac{\sigma_P}{\sqrt{N_{\text{eff}}}}. \quad (18)$$

From (18), we see that $1/\sqrt{N_{\text{eff}}}$ is directly proportional to the standard error in an estimate of the mean power and is thereby a measure of the uncertainty in the average power estimate, \hat{P} .

Normalizing $\sigma_{\hat{P}}$ by the average power \bar{P} and recognizing that $\sigma_P = \bar{P}$ for the exponentially distributed random variable P considered here, we find that the *relative standard error*, denoted RSE, is given by

$$\text{RSE} = \frac{\sigma_{\hat{P}}}{\bar{P}} = \frac{1}{\sqrt{N_{\text{eff}}}}. \quad (19)$$

B. Data Standardization

The row standardization introduced in Section IV to mitigate the effects of calculating the correlation matrix over some bandwidth will reduce the column rank of the data matrix \mathbf{H} by one. This rank reduction leads to an underestimation of the dataset's effective number of uncorrelated measurements. This may be easily compensated by observing that reducing the column rank of \mathbf{H} by one will likewise reduce N_{eff} by one. Thus, for a row standardized data matrix \mathbf{H} , the actual value of N_{eff} is given by

$$N'_{\text{eff}} = N_{\text{eff}} + 1. \quad (20)$$

For the sake of simplicity, the term ‘‘effective number of uncorrelated measurements,’’ N_{eff} , will henceforth refer to the primed variable given in (20).

C. Application to Reverberation Chamber Measurements

The accuracy of the effective number of uncorrelated measurements depends heavily on the accuracy of the estimated correlation matrix and thereby, the underlying covariance matrix. Furthermore, whereas the accuracy of individual elements of the correlation matrix depend purely on the number of observations (frequencies) M' , the summation in (12) reveals that the accuracy of N_{eff} , also depends on the number of variables (stirrer positions) N . To minimize this error, we use improved covariance matrix estimators that are more accurate than the sample covariance matrix for smaller ratios of M'/N .

In Appendix B, we demonstrate the importance of these improved covariance matrix estimators via a brief study of the sensitivity of N_{eff} to M'/N for a range of N . Based on this study and recognizing that the calculation bandwidth is given by $M'B_c$, where B_c is the chamber's loading-dependent coherence bandwidth, we determined that a 1 GHz calculation bandwidth was sufficient to ensure that the relative uncertainty in N_{eff} was less than 5% for the case of $N \leq 360$ measurements

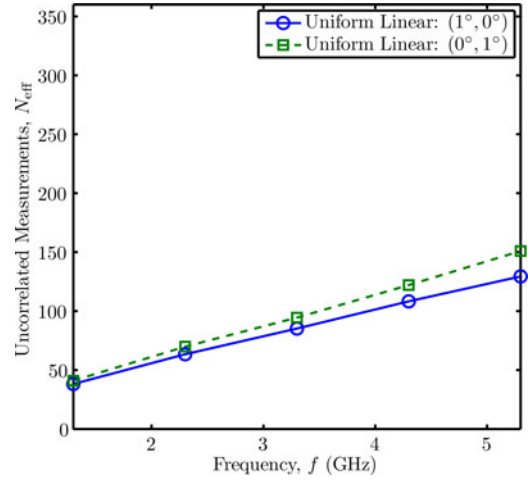


Fig. 6. Effective number of uncorrelated measurements, N_{eff} , for $N = 360$ measurements.

and three absorbers as well as $N \leq 100$ measurements with five absorbers. This covered the majority of the N_{eff} -based analyses to be presented here. Based on our discussion of the correlation matrix in Section IV, we expect that using a frequency-averaged correlation matrix will result in an effective number of uncorrelated measurements that corresponds roughly to the calculation bandwidth's center. This is partially confirmed by Appendix B's analysis of the sensitivity of N_{eff} to M and N , wherein we observed little change in the asymptotic value of N_{eff} for order-of-magnitude changes in the calculation bandwidth. Finally, we note that we purposefully used the sample covariance matrix for our analysis in Section IV, because it results in an unbiased correlation matrix estimate better suited for qualitative analysis of structural details. Here, in contrast, our analysis is more quantitative and thus requires a more accurate correlation matrix estimate.

Fig. 6 presents example calculations of the effective number of uncorrelated measurements N_{eff} for the same two sets of $N = 360$ measurements as were considered in Fig. 4 for the estimated number of uncorrelated measurements N_{est} based on the autocovariance's coherence angle, ϕ_c . Similar to N_{est} in Fig. 4, N_{eff} in Fig. 6 was calculated at 1 GHz increments by use of measurement data within a 1 GHz bandwidth. We see that both N_{eff} and N_{est} in Figs. 4 and 6 exhibit similar trends. We also see that N_{est} based on a stirrer autocorrelation's full-width at half-maximum coherence angle tends to underestimate the effective number of uncorrelated measurements, N_{eff} , by about 33%. This suggests that N_{est} may be more accurate if the coherence angle ϕ_c is determined by use of an autocovariance threshold greater than 0.5.

We note that of all the correlation metrics considered here, it is only possible to quantitatively compare N_{eff} and N_{est} , because they are the only two metrics with identical dimensions (scalar) and units (number of measurements). However, even this comparison is extremely limited, because, as was noted in Section III, calculating N_{est} requires a finely sampled stirrer autocorrelation for determining the threshold-based coherence angle. In contrast, N_{eff} , which is calculated from the data's

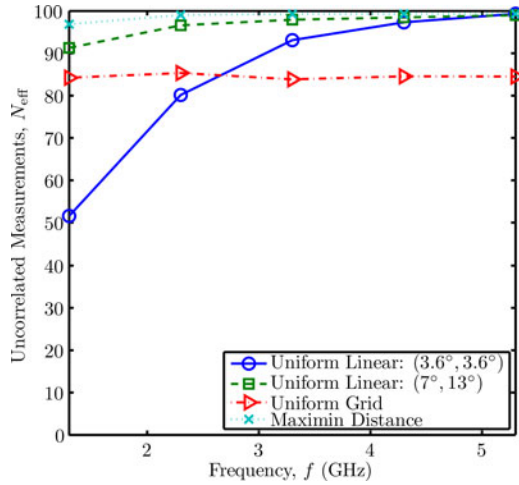


Fig. 7. Effective number of uncorrelated measurements, N_{eff} , for $N = 100$ measurements.

correlation matrix, is applicable regardless of how the data are collected. Furthermore, whereas N_{est} is a premeasurement estimate of how many uncorrelated measurements one might make in a reverberation chamber, N_{eff} is a postmeasurement assessment of the datasets effective number of uncorrelated measurements.

Fig. 7 presents example calculations of N_{eff} for $N = 100$ measurements using different stirrer rotation algorithms and a three-absorber loading configuration. The effective number of uncorrelated measurements was again calculated at 1 GHz increments by use of measurement data within a 1 GHz bandwidth. The “Uniform Linear: $(7^\circ, 13^\circ)$ ” and the “Maximin Distance” algorithms consistently yielded the largest effective number of uncorrelated measurements. This is because both stirrer rotation algorithms are effective at distributing the measurement points in the ϕ_1 - ϕ_2 angle space while also providing a unique set of N stirrer rotation angles for each stirrer. In contrast, the subpar performance of the “Uniform Grid” stirrer rotation algorithm is due to correlation among measurements with identical ϕ_1 or ϕ_2 stirrer angles, as was discussed in Section IV. The poor performance of the “Uniform Linear: $3.6^\circ/3.6^\circ$ ” stirrer rotation algorithm at low frequencies is due to the small stirrer rotation angle of $\Delta\phi = 3.6^\circ$. Reexamining Fig. 3, we see that 3.6° is less than either stirrer’s coherence angle, ϕ_c , for frequencies below about 4.5 GHz.

Fig. 8 presents example calculations of N_{eff} for $N = 100$ measurements obtained using the “Uniform Linear: $(7^\circ, 13^\circ)$ ” stirrer rotation algorithm with different reverberation chamber loading configurations. The effective number of uncorrelated measurements was calculated in the same manner as the N_{eff} presented in the previous figures. Increasing the number of absorbers reduces the chamber’s quality factor, and we note that for NIST’s chamber at 2 GHz, zero, one, three, and five absorbers correspond to quality factors of approximately 2×10^4 , 6×10^3 , 2×10^3 , and 1×10^3 , respectively. As Fig. 8 indicates, this reduced quality factor leads to increased measurement correlation and a reduction in the dataset’s effective number of uncorrelated measurements, N_{eff} .

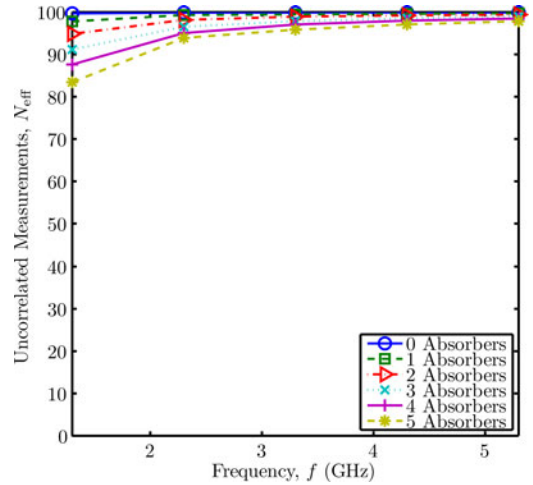


Fig. 8. Effective number of uncorrelated measurements, N_{eff} , for different loading configurations with $N = 100$ and $(7^\circ, 13^\circ)$ stirrer steps.

To confirm that the observed dependence of N_{eff} on loading is due to increased correlation between measurements and not the loading-dependent number of uncorrelated frequencies M' in the 1 GHz calculation bandwidth, we repeated the calculations using a 500 MHz calculation bandwidth. Despite halving M' , we observed a maximum change in N_{eff} of 1.5%, with typical changes of less than 0.5%. This indicates that the observed differences in N_{eff} for different loadings is dominated by measurement correlation effects and also demonstrates the robustness of the improved covariance matrix estimators used in the calculation of N_{eff} .

VI. MEASUREMENT EFFICIENCY

The effective number of uncorrelated measurements, N_{eff} , quantifies the amount of unique information that was obtained from the N measurements. By normalizing N_{eff} by N , we arrive at an alternative metric that succinctly summarizes how efficiently our measurement methodology acquires this information. We define this *measurement efficiency*, $\varepsilon_N \in [0, 1]$, as

$$\varepsilon_N = \frac{N_{\text{eff}}}{N}. \quad (21)$$

For reverberation chamber measurements, ε_N reveals the effectiveness of a given stirring technique for a given loading and/or antenna configuration. A measurement efficiency approaching unity indicates a highly effective stirring technique that yields uncorrelated measurements, whereas a measurement efficiency approaching zero indicates a poor stirring technique wherein improvements could be made. We note a quantity similar to ε_N has been used extensively in quantum chemistry to describe the *participation ratio* or *spatial filling factor* of an orbital [32], [35].

Fig. 9 presents example calculations of measurement efficiency, ε_N , versus the number of measurements, N , for reverberation chamber datasets obtained by use of the “Uniform Linear: $(8.5^\circ/11.5^\circ)$ ” stirrer rotation algorithm with different loading configurations. Due to the larger values of N considered

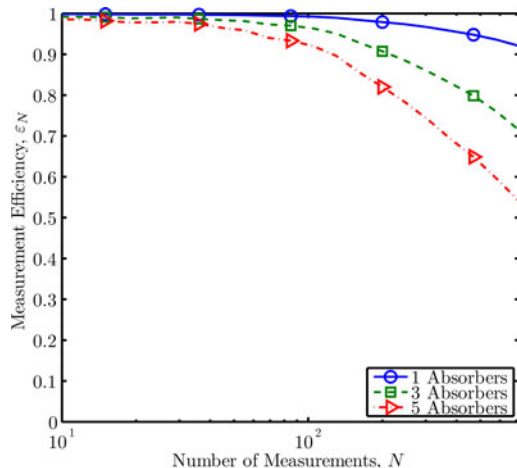


Fig. 9. Measurement efficiency, ε_N , versus number of measurements, N , for different loading configurations using the $8.5^\circ/11.5^\circ$ uniform linear stirrer rotation algorithm.

here—up to 720—we calculate the effective number of uncorrelated measurements, N_{eff} , from a 2 GHz bandwidth centered about 2 GHz so as to ensure a relative uncertainty of less than 5%. Examining Fig. 9, we observe that as the number of measurements, N , increases, the measurement efficiency, ε_N , decreases. This is because as N increases, the measurement points are more densely packed into the ϕ_1 - ϕ_2 angle space. This tighter packing leads to greater correlation between measurement that reduces both the effective number of uncorrelated measurements and the measurement’s efficiency. In other words, Fig. 9 indicates that increasing the number of measurements has diminishing returns whereby a small increase in N_{eff} can require a large increase in N .

To understand the implications of the diminishing returns of increasing N , let us consider the uncertainty in a reverberation chamber’s average power measurement as given by the relative standard error, RSE. We assume the chamber is well-stirred, whereby the power is exponentially distributed and $\text{RSE} = 1/\sqrt{N_{\text{eff}}}$ per (19). Fig. 10 examines the relationships between N and RSE for the data presented in Fig. 9. The lower trace gives the lower bound for RSE and corresponds to the case where $N_{\text{eff}} = N$, i.e., where all N measurements are uncorrelated. As may be seen, the three upper traces gradually deviate from the ideal case with increasing N , and the effect is more severe for heavier loading configurations. Similar to the measurement efficiency curves in Fig. 9, Fig. 10 shows that increasing the number of measurements, N , yields diminishing returns on measurement uncertainty. Thus, we observe that correlation among reverberation chamber measurements can hinder efforts to attain measurement uncertainties below target levels, particularly for low quality factor reverberation chambers.

To clearly demonstrate this point, we used N_{eff} to compare two reverberation chamber measurement datasets collected with a five absorber loading configuration. The first dataset used the maximin distance stirrer rotation algorithm to collect $N = 1080$ measurements and yielded $N_{\text{eff}} = 418$ effectively uncorrelated measurements; the second dataset used the uniform grid stirrer

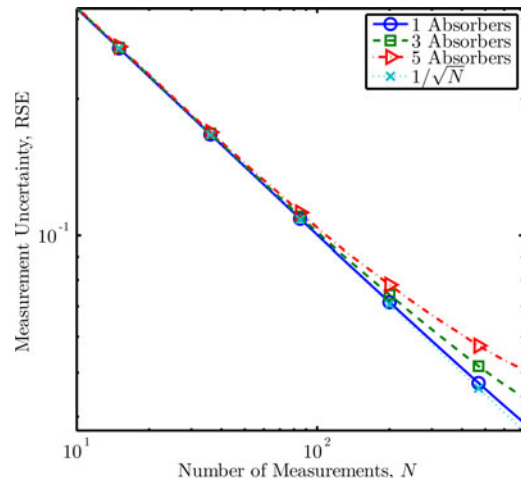


Fig. 10. Relative standard error, RSE, of a power ensemble average for datasets with different number of measurements, N , obtained by use of the $8.5^\circ/11.5^\circ$ uniform linear stirrer rotation algorithm with different loading configurations.

rotation algorithm with $N = 1296$ measurements and yielded $N_{\text{eff}} = 370$ effectively uncorrelated measurements¹. That is, despite collecting 20% more measurements, the uniform grid stirrer rotation algorithm yielded fewer effectively uncorrelated measurements than the maximin distance stirrer rotation algorithm! This clearly demonstrates the increased cost associated with an inefficient measurement methodology.

VII. DISCUSSION

A well-designed reverberation chamber experiment should enable target measurement uncertainty levels to be reached at minimum “cost”. For our discussion, we associate the cost of a measurement with measurement time, and thereby the number of measurements N required to reach the uncertainty target. In this sense, an optimized reverberation chamber measurement methodology should seek to maximize measurement efficiency ε_N such that for a given number of measurements N , one attains the best possible measurement uncertainty at minimum cost. The most direct route to maximizing measurement efficiency is by identifying and mitigating measurement correlation.

As a first step, one should evaluate the autocovariance of individual stirrers so as to determine their corresponding coherence angle/distance. Using (4), this enables an order-of-magnitude estimate of the number of uncorrelated measurements that one may collect and thereby provides insight into the expected measurement uncertainty that may be attained for a given chamber. More importantly, this coherence metric quantitatively evaluates the performance of each stirrer and provides a key input parameter for designing an effective stirring methodology, which, as evidenced by Figs. 5 and 7, is critical for minimizing measurement correlation.

¹To ensure accuracy in the calculations of N_{eff} for the large N , the datasets’ correlation matrices were calculated from a 4 GHz bandwidth centered about 3.5 GHz.

Based on our experience with the maximin distance algorithm, which consistently exhibited the best performance of the three algorithms considered here, we expect that a “good” stirrer rotation algorithm should uniformly distribute the measurement points in angle space while ensuring that all stirrer angles are unique for each measurement. Additionally, the algorithm should ensure that for any two measurement points, their separation in at least one dimension (e.g., ϕ_1 or ϕ_2) is equal to or greater than the corresponding stirrer’s coherence angle/distance. This allows for similar albeit still unique stirrer angles for one stirrer at a time and relies on the other stirrer(s) to de-correlate the measurements. Ideally, we would like the separation between measurement points in *all* dimensions to exceed the corresponding stirrers’ coherence angle/distance metrics, but this can be impractical, because it severely restricts the number of measurements that one may collect.

As Figs. 8–10 showed, reducing the chamber loading will increase the effective number of uncorrelated measurements and thereby improve measurement efficiency. For those using reverberation chambers with intrinsically low quality factors, additional stirrers or stirring techniques (e.g., frequency, polarization, or platform stirring) are likely invaluable for reducing the measurement correlation and thereby improving measurement efficiency. Otherwise, they may find that an exorbitant number of measurements are required to meet the target measurement uncertainty criterion. This is evidenced by the aforementioned auxiliary study, wherein $N = 1080$ measurements (obtained using the maximin distance stirrer rotation algorithm) were required to attain a relative standard error of $1/\sqrt{N_{\text{eff}}} = 1/\sqrt{418} \approx 5\%$ for a five absorber loading configuration.

VIII. CONCLUSION

Correlation impairs both the efficiency and accuracy of reverberation chamber measurements and should thus be mitigated whenever possible. As noted throughout our discussion, the different metrics serve different purposes. The autocovariance is useful for evaluating the effectiveness of an individual stirrer, and the corresponding minimum stepsize provides information invaluable to measurement planning. Correlation matrices provide a comprehensive picture of measurement correlation that may be used to qualitatively assess different stirring methodologies as well as develop new stirring methodologies with minimum correlation between measurements. Finally, the succinct entropy-based metrics enable quantitative comparisons of the performance of different measurement methodologies. These metrics will not only prove useful for optimizing one’s measurement methodology as discussed in Section VII, but are also expected to facilitate the development and validation of theoretical bounds on a given chamber’s measurement uncertainty.

Using several correlation metrics, it was shown that measurement correlation is strongly affected by the stirring methodology, the chamber loading configuration, and the measurement frequency. For many scenarios, the measurement frequency as well as the reverberation chamber’s quality factor will be fixed. Thus, for a given reverberation chamber, the only way to reduce correlation among measurements is by maximizing the unique-

ness of each measurement’s stirrer position(s). This suggests that an optimized stirring methodology is critical for realizing uncorrelated measurements.

It is conceivable that numerous other measurement parameters such as chamber dimensions, stirrer geometries, antenna patterns, orientations, and polarizations, etc., affect measurement correlation, whereby a complete guide to minimizing measurement correlation will require a far more comprehensive study than that presented here. These investigations will be the focus of future studies, but importantly, the analyses described herein enable the objective comparisons necessary for discerning which measurement parameters are critical for maximizing measurement efficiency.

APPENDIX A

MAXIMIN DISTANCE STIRRER ROTATION ALGORITHM

We begin by defining Φ_1 as the ordered set of $N > 1$ angles for the first stirrer as

$$\Phi_1 = \left\{ 0^\circ, \frac{360^\circ}{N}, 2\frac{360^\circ}{N}, \dots, (N-1)\frac{360^\circ}{N} \right\}. \quad (22)$$

Thus, Φ_1 is a sequence of N angles equispaced from 0° to 360° . The maximin distance algorithm defines the N angles for the second stirrer as a permutation of Φ_1 . Denoting the second stirrer’s ordered set of N angles as Φ_2 , the bijective mapping of the N -element sequence Φ_1 to the N -element sequence Φ_2 is given by

$$\Phi_2[A_i] = \Phi_1[i] \quad (23)$$

where $i, A_i \in \{1, 2, \dots, N\}$ and A_i is the i th element of the sequence A that is itself the concatenation of K sequences, $A^{(k)}$ of the form

$$A^{(k)} = \{A_i^{(k)} | A_i^{(k)} = k + (i-1)K \text{ and } A_i^{(k)} \leq N\}. \quad (24)$$

The K sequences $A^{(k)}$ are ordered such that A is given by

$$A = \{A^{(B_1)}, A^{(B_2)}, \dots, A^{(B_K)}\} \quad (25)$$

where B_j denotes the j th element of the auxiliary sequence B given by

$$B = \left\{ 1, 1 + \left\lceil \frac{K}{2} \right\rceil, 2, 2 + \left\lceil \frac{K}{2} \right\rceil, \dots \mid B_j \leq K \right\} \quad (26)$$

with $j \in \{1, 2, \dots, K\}$ and $\lceil \cdot \rceil$ denoting the ceiling function that rounds up to the nearest integer.

The permutation parameter K used in Eqs. (25)–(26) is in general given by

$$K = \left\lceil \sqrt{N} \right\rceil \quad (27)$$

where $\lceil \cdot \rceil$ denotes the rounding function, which rounds to the nearest integer. However, for select values of N , K will generate a permutation such that there are pairs of measurement points in the ϕ_1 - ϕ_2 angle space whose separation distance in both ϕ_1 and

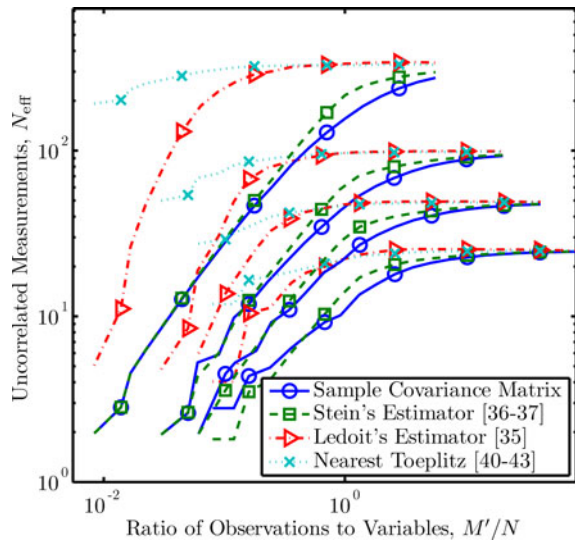


Fig. 11. Behavior of N_{eff} calculated by use of different covariance matrix estimators with different number of measurements, N , and different observation-to-variable ratios, M'/N , by use of the $7^\circ/13^\circ$ uniform linear stirrer rotation algorithm and a three absorber loading configuration.

ϕ_2 is $360^\circ/N$. That is, these points will be minimally separated in angle space. Provided that $N \notin \{2, 4, 8\}$, these cases may be resolved by substituting for K the alternative permutation parameter K' given by

$$K' = \lceil \sqrt{N} \rceil + 1 - 2\lceil \sqrt{N} \bmod 1 \rceil \quad (28)$$

where $y \bmod x$ denotes the modulo operator that yields the remainder of y/x . The following are three special cases where K' should be used in place of K so as to generate the most effective permutation:

- 1) \sqrt{N} is an even integer.
- 2) K is an even integer and N/K is integer.
- 3) K is an odd integer and $\frac{2N-K-1}{2K}$ is an integer.

APPENDIX B

UNCERTAINTY IN N_{eff}

Generally, the error in the sample covariance matrix manifests itself as an overestimation of the off-diagonal matrix elements [36] which, from (5) and (12), will lead to an underestimation of a dataset's effective number of uncorrelated measurements. The majority of the improved covariance matrix estimators either 1) seek to compensate for the sample covariance matrix's overestimation of its off-diagonal elements [36]–[38], [38], or 2) impose some predetermined structure on the covariance matrix estimate [39], [40].

Fig. 11 compares the effective number of uncorrelated measurements, N_{eff} , about a center frequency of 3.5 GHz as calculated by use of several covariance matrix estimators for different number of measurements N and uncorrelated frequencies M' by use of the “Uniform Linear: (7° , 13°)” stirrer rotation algorithm. The curves in Fig. 11 indicate that N_{eff} based on the different covariance matrix estimators tend to approach the same value with increasing M'/N . However, the rate at which these differ-

ent estimators approach the asymptotic limit depends on both the number of measurements, N , and the ratio of observations to variables, M'/N . From Fig. 11, we see that N_{eff} calculated from the Toeplitz covariance matrix estimator tends to approach this asymptotic value the most rapidly. This motivated our decision to use structured covariance wherever possible, as noted in Section V.

For calculations of N_{eff} in this paper, Ledoit's shrinkage-based covariance matrix estimator [36] was used with data collected by use of the maximin distance stirrer rotation algorithm; for all other datasets, an appropriate structured covariance matrix estimator was used [40]. Specifically, a Toeplitz covariance matrix estimator was used with data collected by way of the uniform linear stirrer rotation algorithm unless $\Delta\phi_1 = 360^\circ/N$ and $\phi_2 = 0^\circ$, $\Delta\phi_2 = 360^\circ/N$ and $\phi_1 = 0^\circ$, or $\Delta\phi_1 = \Delta\phi_2 = 360^\circ/N$; for these cases, a circulant covariance matrix estimator was used. For data collected by way of the uniform grid stirrer rotation algorithm, a circulant block-circulant covariance matrix estimator was used. These structured covariance matrices were found by first using the efficient albeit crude projection technique [41], [42] and then taking the nearest positive semidefinite matrix as described in [43], [44] to ensure a valid covariance matrix.

Based on Fig. 11 and similar unreported analyses for the other stirrer rotation algorithms, we conclude that the empirical N_{eff} reported in this paper have a relative uncertainty of less than 5%. This uncertainty accounts for the possible error in N_{eff} due to finite values of M'/N for various N . Other uncertainties (e.g., due to measurement noise) are expected to be negligible in comparison.

Finally, we recognize that this analysis of the uncertainty in N_{eff} is complicated by the measurement data's frequency-dependent correlation, whereby measurements at lower frequencies tend to be more correlated than those at higher frequencies (see Figs. 4 and 6). Discerning the impact of this frequency-dependent correlation on the calculation of N_{eff} is difficult, because the additional frequencies are necessary to accurately estimate the data's covariance matrix. However, Fig. 11 suggests that the net effect of this frequency-dependent correlation on N_{eff} may be small, possibly because the higher correlation at low frequencies is offset by the lower correlation at high frequencies.

REFERENCES

- [1] K. Rosengren and P.-S. Kildal, “Radiation efficiency, correlation, diversity gain, and capacity of a six-monopole antenna array for a MIMO system: Theory, simulation, and measurement in reverberation chamber,” *IEEE Proc.-Microw. Antennas Propag.*, vol. 152, no. 1, pp. 7–16, Feb. 2005.
- [2] M. L. Crawford and G. H. Koepke, “Design, evaluation, and use of a reverberation chamber for performing electromagnetic susceptibility/vulnerability measurements,” Nat. Bur. Stand. (U.S.), Tech. Note 1092, 1986.
- [3] C. Orlenius, P.-S. Kildal, and G. Poilasne, “Measurements of total isotropic sensitivity and average fading sensitivity of CDMA phones in reverberation chamber,” in *Proc. IEEE AP-S Int. Symp.*, vol. 1, Washington, DC, Jul. 3–8, 2005, pp. 409–412.
- [4] J. F. Valenzuela-Valdés, M. A. García-Fernández, A. M. Martínez-Gonzalez, and D. A. Sánchez-Hernández, “The influence of efficiency on receive diversity and MIMO capacity for Rayleigh-fading channels,” *IEEE Trans. Antennas Propag.*, vol. 56, no. 5, pp. 1444–1450, May 2008.

- [5] S. J. Floris, K. A. Remley, and C. L. Holloway, "Bit error rate measurements in reverberation chambers using real-time vector receivers," *IEEE Antennas Wireless Propag. Lett.*, vol. 9, pp. 619–622, 2010.
- [6] E. Genender, C. L. Holloway, K. A. Remley, J. Ladbury, and G. Koepke, "Simulating the multipath channel with a reverberation chamber: Application to bit error measurements," *IEEE Trans. Electromagn. Compat.*, vol. 52, no. 4, pp. 766–777, 2010.
- [7] K. Rosengren, P.-S. Kildal, C. Carlsson, and J. Carlsson, "Characterization of antennas for mobile and wireless terminals in reverberation chambers: Improved accuracy by platform stirring," *Microw. Opt. Technol. Lett.*, vol. 30, no. 6, pp. 391–397, Sep. 2001.
- [8] K. Madsén, P. Hallbjörner, and C. Orlenius, "Models for the number of independent samples in reverberation chamber measurements with mechanical, frequency, and combined stirring," *IEEE Antenn. Propagat. Lett.*, vol. 3, pp. 48–51, 2004.
- [9] J. Clegg, A. C. Marvin, J. F. Dawson, and S. J. Porter, "Optimization of stirrer designs in a reverberation chamber," *IEEE Trans. Electromagn. Compat.*, vol. 47, no. 4, pp. 824–832, Nov. 2005.
- [10] C. Lemoine, P. Besnier, and M. Drissi, "Estimating the effective sample size to select independent measurements in a reverberation chamber," *IEEE Trans. Electromagn. Compat.*, vol. 50, no. 2, pp. 227–236, May 2008.
- [11] O. Lundén and M. Bäckström, "Stirrer efficiency in FOA reverberation chambers: Evaluation of correlation coefficients and chi-squared tests," in *IEEE Int. Symp. Electromagn. Compat.*, 2000, Aug. 21–25, 2000, vol. 1, pp. 11–16.
- [12] P. Hallbjörner, "Estimating the number of independent samples in reverberation chamber measurements from sample differences," *IEEE Trans. Electromagn. Compat.*, vol. 48, no. 2, pp. 354–358, May 2006.
- [13] N. Wellander, O. Lundén, and M. Bäckström, "Experimental investigation and mathematical modeling of design parameters for efficient stirrers in mode-stirred reverberation chambers," *IEEE Trans. Electromagn. Compat.*, vol. 49, no. 1, pp. 94–103, Feb. 2007.
- [14] L. R. Arnaut, "Uncertainty reduction and decorrelation of mode-stirred reverberation chamber data using transformation and expansion techniques," Nat. Phys. Lab, Middlesex, U.K., Tech. Rep. CETM 21, Jun. 2000.
- [15] L. R. Arnaut, "Effect of local stir and spatial averaging on measurement and testing in mode-tuned and mode-stirred reverberation chambers," *IEEE Trans. Electromagn. Compat.*, vol. 43, no. 3, pp. 305–325, Aug. 2001.
- [16] C. L. Holloway, D. A. Hill, M. Sandroni, J. M. Ladbury, J. S. Coder, G. Koepke, A. C. Marvin, and Y. He, "Use of reverberation chambers to determine the shielding effectiveness of physically small, electrically large enclosures and cavities," *IEEE Trans. Electromagn. Compat.*, vol. 50, no. 4, pp. 770–782, Nov. 2008.
- [17] K. G. Beauchamp and C. K. Yuen, *Digital Methods for Signal Analysis*. Crows Nest, New South Wales, U.K.: George Allen & Unwin Ltd., 1976.
- [18] C. L. Holloway, D. A. Hill, J. M. Ladbury, P. F. Wilson, G. Koepke, and J. Coder, "On the use of reverberation chambers to simulate a Rician radio environment for the testing of wireless devices," *IEEE Antennas Propag.*, vol. 11, no. 11, pp. 3167–3177, Nov. 2006.
- [19] O. Delangre, P. D. Doncker, M. Lienard, and P. Degauque, "Analytical angular correlation function in mode-stirred reverberation chamber," *Electron. Lett.*, vol. 45, no. 2, pp. 90–91, 2009.
- [20] D. F. Morrison, *Multivariate Statistical Methods*. New York: McGraw-Hill, 1967.
- [21] K. A. Remley, S. J. Floris, H. A. Shah, and C. L. Holloway, "Static and dynamic propagation channel impairments in reverberation chambers," *IEEE Trans. Electromagn. Compat.*, vol. PP, pp. 1–11, 2011.
- [22] H. Hotelling, "New light on the correlation coefficient and its transforms," *J. R. Statist. Soc. Series B (Methodol.)*, vol. 15, no. 2, pp. 193–232, 1953.
- [23] E. P. P. Corona and G. Latmiral, "Performance and analysis of a reverberating enclosure with variable geometry," *IEEE Trans. Electromagn. Compat.*, vol. 22, no. 1, pp. 2–5, Feb. 1980.
- [24] J. S. Hair, Jr, W. C. Black, R. E. Anderson, and R. L. Tatham, *Multivariate Data Analysis*, 6th ed. Upper Saddle River, NJ: Pearson Education, Inc., 2006.
- [25] B. Efron, "Are a set of microarrays independent of each other?" *Ann. Appl. Statist.*, vol. 3, no. 3, pp. 922–942, 2009.
- [26] J. V. Neumann, *Mathematical Foundations of Quantum Mechanics*. Princeton, NJ: Princeton University, 1955.
- [27] C. S. Bretherton, M. Widmann, V. P. Dymnikov, J. M. Wallace, and I. Bladé, "The effective number of spatial degrees of freedom of a time-varying field," *J. Climate*, vol. 12, no. 7, pp. 1990–2009, Jul. 1999.
- [28] K. Fraedrich, C. Ziehmann, and F. Sielmann, "Estimates of the spatial degrees of freedom," *J. Climate*, vol. 8, no. 2, pp. 361–369, Feb. 1995.
- [29] M. Righero, O. D. Feo, and M. Biey, "A cooperation index based on correlation matrix spectrum and Rényi entropy," in *Proc. Eur. Conf. Circuit Theory Design, 2009*, Antalya, Turkey, Aug. 23–27, 2009, pp. 466–469.
- [30] A. Rényi, "On measures of entropy and information," in *Proc. 4th Berkeley Symp. Math. Statist. Prob.*, vol. 1. Berkeley, CA: Univ. California Press, 1961, pp. 547–561.
- [31] K. Życzkowski, "Rényi extrapolation of Shannon entropy," *Open Syst. Inf. Dyn.*, vol. 10, no. 3, pp. 297–310, Sep. 2003.
- [32] I. Varga and J. Pipek, "On Rényi entropies characterizing the shape and the extension of the phase space representation of quantum wave functions in disordered systems," *Phys. Rev. E*, vol. 68, no. 2, p. 026202, Aug. 2003.
- [33] R. K. Mallik, "On multivariate Rayleigh and exponential distributions," *IEEE Trans. Inf. Theory*, vol. 49, no. 6, pp. 1499–1515, Jun. 2003.
- [34] R. M. Mickey, O. J. Dunn, and V. A. Clark, *Applied Statistics: Analysis of Variance and Regression*, 3rd ed. Hoboken, NJ: Wiley, 2004.
- [35] J. Pipek and I. Varga, "Universal classification scheme for the spatial-localization properties of one-particle states in finite, d -dimensional systems," *Phys. Rev. A*, vol. 46, no. 6, pp. 3148–3163, Sep. 1992.
- [36] O. Ledoit and M. Wolf, "A well-conditioned estimator for large-dimensional covariance matrices," *J. Multivariate Anal.*, vol. 88, no. 2, pp. 365–411, Feb. 2004.
- [37] D. K. Dey and C. Srinivasan, "Estimation of a covariance matrix under Stein's loss," *Ann. Statist.*, vol. 13, no. 4, pp. 586–597, Dec. 1985.
- [38] R. J. Muirhead, "Developments in Eigenvalue Estimation," in *Advances in Multivariate Statistical Analysis*. Boston, MA: D. Reidel Publishing Co., 1987, pp. 277–288.
- [39] T. A. Barton and D. R. Fuhrmann, "Covariance structures for multidimensional data," in *Conf. Record 25th Asilomar Conf. Signals, Syst., Comput.*, Pacific Grove, CA, Nov. 4–6, 1991, vol. 1, pp. 297–301.
- [40] A. J. Storkey, "Truncated covariance matrices and Toeplitz methods in Gaussian processes," in *Proc. 9th Int. Conf. Neural Netw.*, Edinburgh, U.K., Sep. 7–10, 1999, vol. 1, pp. 55–60.
- [41] D. M. Wilkes and M. H. Hayes, "Iterated Toeplitz approximation of covariance matrices," in *Proc. Int. Conf. Acoust., Speech, Signal Process.*, New York, NY, Apr. 11–14, 1988, vol. 3, pp. 1663–1666.
- [42] T. A. Barton and S. T. Smith, "Structured covariance estimation for space-time adaptive processing," in *Proc. IEEE Int. Conf. Acoust., Speech, Signal Process.*, Munich, Germany, Apr. 21–24, 1997, vol. 5, pp. 3493–3496.
- [43] N. J. Higham, "Computing a nearest symmetric positive semidefinite matrix," *Linear Algebra Appl.*, vol. 103, pp. 103–118, 1988.
- [44] N. J. Higham, "Matrix nearness problems and applications," in *Proc. IMA Conf. Appl. Matrix Theory*, M. J. C. Gover and S. Barnett, Eds. London, U.K.: Oxford Univ. Press, 1989, pp. 1–27.



Ryan J. Pirkl (S'06–M'10) received the B.S., M.S., and Ph.D. degrees in electrical engineering from the Georgia Institute of Technology, in Atlanta, Georgia, in 2005, 2007, and 2010, respectively. For his graduate research, he developed hardware measurement procedures, and processing tools for in situ characterization of radio wave propagation mechanisms.

In 2010, he began working at the National Institute of Standards and Technology in Boulder, CO, under a National Research Council Postdoctoral Research Associateship. He is currently investigating how reverberation chambers may be used as tunable wireless channel emulators for wireless device testing. His research interests include reverberation chambers, radio wave propagation, and analytical electromagnetics.



Kate A. Remley (S'92–M'99–SM'06) was born in Ann Arbor, MI. She received the Ph.D. degree in electrical and computer engineering from Oregon State University, Corvallis, in 1999.

From 1983 to 1992, she was a Broadcast Engineer in Eugene, OR, serving as Chief Engineer of an AM/FM broadcast station from 1989–1991. In 1999, she joined the Electromagnetics Division of the National Institute of Standards and Technology (NIST), Boulder, CO, as an Electronics Engineer.

Her research activities include metrology for wireless systems, characterizing the link between nonlinear circuits and system performance, and developing methods for improved radio communications for the public-safety community.

Dr. Remley was the recipient of the Department of Commerce Bronze and Silver Medals and an ARFTG Best Paper Award. She is currently the Editor-in-Chief of IEEE Microwave Magazine and Immediate Past Chair of the MTT-11 technical committee on microwave measurements.



Christian S. Lötback Patané received the B.S. and M.S. degrees in Engineering Physics from Chalmers University of Technology in Gothenburg, Sweden, in 2008 and 2010, respectively. For his Master's thesis work, he studied reverberation chamber measurement uncertainties and parameter estimations at the National Institute of Standards and Technology in Boulder, Colorado.

In 2010, he began working at Bluetest, which is a company situated in Gothenburg, Sweden, that develops and manufactures reverberation chambers for commercial use. Currently, he is working as an R&D engineer, developing hardware and measurement procedures for the reverberation chamber. He is also participating in standard organizations, such as CTIA and 3GPP, as a reverberation chamber expert.